

1 **A global analysis of reconstructed land climate changes during Dansgaard-** 2 **Oeschger events**

3 Mengmeng Liu^{1,2,*}, Iain Colin Prentice¹, Sandy P. Harrison²

4 1: Georgina Mace Centre for the Living Planet, Department of Life Sciences, Imperial College
5 London, Silwood Park Campus, Buckhurst Road, Ascot SL5 7PY, UK

6 2: Department of Geography and Environmental Science, University of Reading, Reading,
7 RG6 6AB, UK

8 *** Corresponding author: m.liu18@imperial.ac.uk**

9 Ms for: *Climate of the Past*

10 **Abstract**

11 Dansgaard–Oeschger (D–O) warming events are comparable in magnitude and rate to the
12 anticipated 21st century warming. As such, they provide a good target for evaluation of the
13 ability of state-of-the-art climate models to simulate rapid climate changes. Despite the wealth
14 of qualitative information about climate changes during the D–O events, there has been no
15 attempt to date to make quantitative reconstructions globally. Here we provide reconstructions
16 of seasonal temperature changes and changes in plant-available moisture across multiple D–O
17 events during Marine Isotope Stage 3 based on available pollen records across the globe. These
18 reconstructions show that the largest warming occurred in northern extratropics, especially
19 Eurasia, while western North America and the southern extratropics were characterised by
20 cooling. The change in winter temperature was significantly larger than the change in summer
21 temperature in the northern extratropics, indicating that the D–O warming events were
22 characterised by reduced seasonality, but there is no significant difference between the summer
23 and winter temperature changes in the southern extratropics. The antiphasing between northern
24 and southern extratropical changes, and the west-east pattern of cooling and warming in North
25 America are consistent across the eight D–O events examined, although the signal at individual
26 sites may vary between events. Globally, changes in moisture were positively correlated with
27 changes in temperature, but the strength and the sign of this relationship vary regionally. These
28 reconstructions can be used to evaluate the spatial patterns of changes in temperature and

- 29 moisture in the transient simulations of the D-O events planned as part of the Palaeoclimate
30 Modelling Intercomparison Project.

31 1. Introduction

32 Dansgaard–Oeschger (D–O) events are characterised in Greenland by a transition from cold
33 Greenland Stadial (GS) to warmer Greenland Interstadial (GI) conditions (Dansgaard et al.,
34 1993). The surface air temperature in Greenland increased by 10–15° C during the warming
35 phases; these warming events occur over an interval of between 50 and 200 years (Huber et
36 al., 2006; Kindler et al., 2014). Thus, the D-O events offer a parallel in terms of speed to
37 projected future warming, although both the baseline state and the mechanism inducing this
38 warming differ from anticipated 21st century climate changes. D-O events could therefore
39 provide an opportunity to determine how well climate models that are used for future
40 projections can simulate rapid climate changes (Malmierca-Vallet et al., 2023), particularly
41 regional patterns of warming (and cooling) that are regarded as a challenge for modelling
42 (Doblas-Reyes et al., 2021; Lee et al., 2021) and are highly important in assessing the
43 vulnerability of human societies to future climate changes (IPCC 2022).

44 D-O events are registered globally (Voelker, 2002; Sánchez Goñi and Harrison, 2010; Harrison
45 and Sánchez Goñi, 2010; Sánchez Goñi et al., 2017; Adolphi et al., 2019; Corrick et al., 2020).
46 Shifts in vegetation types between GI and GS states have been interpreted as primarily a
47 temperature signal in the extratropics and a moisture signal in the tropics (Harrison and
48 Sánchez Goñi, 2010). Speleothem records provide a good time-control on the synchronicity of
49 climate changes globally with the D-O events registered in Greenland (Adolphi et al., 2019;
50 Corrick et al., 2020), but the driver of this signal can either be temperature or precipitation
51 depending on the region. There are quantitative climate reconstructions based on terrestrial
52 pollen records from La Grande Pile (Guiot et al., 1993), Lago Grande di Monticchio (Huntley
53 et al., 1999), Padul (Camuera et al., 2022), El Cañizar de Villarquemado (Wei et al., 2021;
54 Camuera et al., 2022) and Lake Ohrid (Sinopoli et al., 2019), marine cores in the western
55 Mediterranean and offshore from Portugal (Sánchez-Goñi et al., 2002), diatom assemblages at
56 Les Echets, France (Ampel et al., 2010), bacterial membrane lipid records from the Eifel region
57 (Zander et al., 2023), isotopic measurements of earthworm calcite from the Rhine Valley
58 (Prud'homme et al., 2022) and clumped isotope measurements on snails in Hungary (Újvári et
59 al., 2021). Aside from the lack of comparable quantitative estimates from outside Europe,
60 differences in the methodology employed and in the specific climate variables reconstructed in
61 each of these studies limits their usefulness for model evaluation. In particular, given that there
62 is still uncertainty as to whether the D-O cycles are characterised by changes in seasonality

63 such that warming events are primarily driven by changes in winter (Flückiger et al., 2008;
 64 Zander et al., 2024), in the regional strength of the warming (Harrison and Sánchez Goñi, 2010)
 65 and how warming relates to changes in moisture (Wei et al., 2021), there is a need for more
 66 systematic reconstruction of seasonal climate changes.

67 In the paper, we provide reconstructions of seasonal temperature changes and changes in plant-
 68 available moisture during the intervals corresponding to D-O warming events in Greenland
 69 during Marine Isotope Stage 3 based on available pollen records globally. We employ a
 70 standard methodology to construct age models for these records, as well as a standard
 71 regression-based approach to make the reconstructions. We analyse the regional patterns to
 72 identify key targets for model evaluation.

73 2. Methods

74 2.1. Data sources

75 Modern pollen data were obtained from version [2-3](#) of the SPECIAL Modern Pollen [Data](#)
 76 [SetDataset](#) ([SMPDSv2SMPDSv3](#): ~~will be publicly available before the next revision of the~~
 77 ~~paper~~ [Villegas-Díaz and Harrison, 2022](#)). This global [data-setdataset](#) contains [26489-24649](#)
 78 ~~modern pollen recordssamples~~ from [18086 different locations](#)~~17827 sites~~. The dataset [was](#)
 79 ~~contains relative abundance records for 4816 pollen taxa~~, created after removing taxa that are
 80 not climatically diagnostic (e.g. obligate aquatics, carnivorous species, cultivated plants). The
 81 [data-setdataset](#) provides several levels of taxonomic aggregation; here we use the most
 82 aggregated level, where woody species were generally combined at genus level and herbaceous
 83 species at sub-family or family level unless they were palynologically distinctive, occupied
 84 distinctive ecological niches and were sufficiently geographically widespread. This
 85 "amalgamated" [data-setdataset](#) contains relative abundance information for [13621338](#) taxa.
 86 These samples were aggregated by [location \(which is](#) longitude, latitude and elevation) in order
 87 to remove duplicates. Counts for *Quercus*, *Quercus* (deciduous) and *Quercus* (evergreen) were
 88 combined because of inconsistent differentiation of *Quercus* pollen in different regional
 89 records. Deciduous and evergreen oaks occupy different areas of climate space, particularly in
 90 terms of seasonal moisture; specifically, evergreen oaks are typically found in areas
 91 characterised by winter rainfall such as the Mediterranean. Nevertheless, since there are other
 92 plant taxa that are similarly diagnostic of such regimes, the amalgamation of *Quercus*
 93 (deciduous) and *Quercus* (evergreen) should not have a major effect on the robustness of our

94 climate reconstructions. We have tested this assumption by making reconstructions based on
 95 all taxa except *Quercus* (Supplementary Materials, Section 4). Taxa that occurred in less than
 96 10 samples in the training ~~data-set~~dataset were not used to make reconstructions because it is
 97 unlikely that the available samples provided a reasonable estimate of the climate space
 98 occupied by these rare taxa (Liu et al., 2020). After the location aggregation and the taxa
 99 filtering, the ~~data-set~~dataset contains information on 18086 samples with relative abundance
 100 information for 607591 individual pollen-taxa from 17547 sites (Figure 1).

101 We have used a global pollen dataset for calibration of the pollen-climate relationships. The
 102 use of a global dataset, rather than region-specific training data, relies on the principle of
 103 phylogenetic niche conservatism (Harvey and Pagel, 1991; Qian and Ricklefs 2004; Wang et
 104 al., 2025), which states that traits tend to remain constant over time and that the climatic niches
 105 of specific genera are also conservative (Harrison et al., 2025). The use of a global dataset for
 106 calibration makes it possible to sample a large range of climates, and thus makes it more likely
 107 that the reconstructions of glacial climates are realistic and not confined to the limited climate
 108 range sampled in any one region (Turner et al., 2020).

109 The SMPDSv3~~2~~ also provides climatic information at each pollen site, specifically the mean
 110 temperature of the coldest month (MTCO), mean temperature of the warmest month (MTWA),
 111 and a plant-available moisture ~~moisture index~~ (α) calculated as the ratio of actual
 112 evapotranspiration to equilibrium evapotranspiration. These bioclimate variables reflect
 113 mechanistically distinct controls on plant growth. α is a transformation of the commonly used
 114 moisture index MI (Supplementary Materials, Section 2), to emphasize the differences at the
 115 dry end of the climate range, which have a more pronounced effect on vegetation distribution
 116 than differences at the wet end (Prentice et al., 2017). ~~We have also checked~~ The climate space
 117 occupied by SMPDSv3 (Figure S1) to make sure that it sampled a reasonable range of global
 118 climate space and therefore will~~should~~ provide robust reconstructions of climate changes under
 119 glacial conditions.

120 The fossil pollen data were obtained from the Abrupt Climate Changes and Environmental
 121 Responses (ACER) database (Sánchez Goñi et al., 2017), which includes 93 records from the
 122 last glacial period (73-15 ka) with sufficient resolution and dating control to detect sub-
 123 millennial scale variability. Here we focus on the 73 records covering most of Marine Isotope
 124 Stage 3 (50-30 ka); 54 of these records are from terrestrial sites and 19 from marine sites

125 (Figure 1; Table 1). The fossil data were taxonomically harmonised to be consistent with the
126 [SMPDSv2SMPDSv3](#).

127 ~~We have used a global pollen dataset for calibration of the pollen-climate relationships. The~~
128 ~~use of a global dataset, rather than region-specific training data, relies on the principle of~~
129 ~~phylogenetic niche conservatism (Harvey and Pagel, 1991; Qian and Ricklefs 2004; Wang et~~
130 ~~al.,2025), which states that traits tend to remain constant over time. This also applies to the~~
131 ~~climate niche (Wiens and Graham, 2005; Wiens et al., 2010; Peterson, 2011; Crisp and Cook,~~
132 ~~2012; Jiang et al., 2023) as evidenced by disjunct distributions of taxa across different~~
133 ~~continents (Yin et al., 2021). Niche conservatism underpins the fact that the modern~~
134 ~~distribution of specific genera can be predicted using climate pollen relationships developed~~
135 ~~from other regions (e.g. Huntley et al., 1989). The use of a global dataset for calibration makes~~
136 ~~it possible to sample a large range of climates, and thus makes it more likely that the~~
137 ~~reconstructions of glacial climates are realistic and not confined to the limited climate range~~
138 ~~sampled in any one region (Turner et al., 2020). We will test whether our reconstructed glacial~~
139 ~~climates exceed the modern climate ranges in its region.~~

140 **2.2. Climate reconstruction method**

141 We used tolerance-weighted Weighted Averaging Partial Least Squares (fx TWA-PLS: Liu et
142 al., 2020; Liu et al., 2023) regression to model the relationships between taxon abundances and
143 individual climate variables in the [SMPDSv2SMPDSv3](#) modern training dataset and then
144 applied these relationships to reconstruct past climate using the fossil assemblages from the
145 ACER database (Figure 2). fx TWA-PLS reduces the tendency of regression methods to
146 compress reconstructions towards the centre of the sampled climate range by applying a
147 sampling frequency correction to reduce the influence of uneven sampling of climate space
148 and weighting the contribution of individual taxa according to their climate tolerances (Liu et
149 al., 2020). Version 2 of fx TWA-PLS (fx TWA-PLS_{v2}, Liu et al., 2023) uses P-splines
150 smoothing to derive the frequency correction and applies this correction both in estimating the
151 climate optima and tolerances, and in the regression itself, producing a further improvement in
152 model performance compared to [fxTWA-PLSv1version1](#) (Liu et al., 2020).

153 ~~We evaluated the fx TWA-PLS_{v2} models by comparing the reconstructions with observations~~
154 ~~using leave-out cross-validation, where one site at a time was randomly selected as a test site~~
155 ~~and sites that are both geographically close (within 50 km horizontal distance from the site)~~

156 and climatically close (within 2% of the full range of each climate variable in the dataset) were
157 also removed from the training set, to prevent redundancy in the climate information from
158 inflating the cross-validation goodness of fit, following Liu et al. (2020). This ensures that we
159 are not just tuning to the training dataset, and that we can reconstruct climates even when the
160 training set does not completely cover the climate to be reconstructed because there are gaps
161 in the climate space. We evaluated the $fxTWA-PLSv2$ models by comparing the reconstructions
162 with observations using leave-out cross-validation, where one site at a time was randomly
163 selected as a test site and sites that are both geographically close (within 50 km horizontal
164 distance from the site) and climatically close (within 2% of the full range of each climate
165 variable in the dataset) were removed from the training set along with this test site, to prevent
166 redundancy in the climate information from inflating the cross-validation goodness of fit,
167 following Liu et al. (2020). By doing so, we are more convinced that we are not just tuning to
168 the training dataset with susceptible ability to predict new stuff, and that we can reconstruct
169 climates even when our training set can't fully cover the climate we want to reconstruct, in
170 other words, there are gaps in the climate space. We selected the last significant number of
171 components (p -value ≤ 0.01) and assessed model performance using the root mean square error
172 of prediction (RMSEP). Compression was assessed using linear regression of the leave-out
173 cross-validated reconstructions on to the climate variable. Reconstructions of MTCO, MTWA
174 and α were made for every sample in each fossil record. Sample specific errors were estimated
175 via bootstrapping, as described in Liu et al. (2020). We corrected for the effect of changes in
176 atmospheric CO₂ on plant water-use efficiency, and hence the reconstructions of α (Figure
177 [S1S2](#)), following Prentice et al. (2022). Appropriate values of CO₂ were taken from the WAIS
178 Divide ice core record (Bauska et al., 2021).

179 **2.3. Age modelling**

180 Although the ACER database provides age models for each pollen record, the resolution of the
181 individual records is variable (mean resolution [4764](#) years) and these models are often
182 imperfectly aligned with the dating of D-O [warming](#) events as recorded in the Greenland ice
183 core, and which have been shown to have a globally synchronous imprint through analysis of
184 speleothem records (Adolphi et al., 2019; Corrick et al., 2020). To create a better alignment,
185 we [kept the original age model for marine sites since they are generally calibrated using the](#)
186 [oxygen isotope records and are therefore more compatible with the ice core records, and](#) used
187 dynamic time warping (DTW: Belman and Kalaba, 1959; Burstyn et al., 2021; [Alshehri et al.,](#)

188 [2019](#)) to adjust the age scale for each individual [terrestrial](#) record (Figure 2). Dynamic time
 189 warping optimises the similarity between two sequences by stretching or compressing one
 190 sequence in the time dimension to match the other. Here, we use simulated mean annual
 191 temperature (MAT) from a transient simulation of the interval 50-30 ka made with the
 192 LOVECLIM model (Menviel et al., 2014) as the reference sequence compared to MAT
 193 calculated as the average of MTCO and MTWA from the individual pollen records. We used
 194 the mid-point between the start dates of each D-O [warming](#) event [as recorded in the Greenland](#)
 195 [ice core](#) (Wolff et al., 2010; converted into AICC2012 timescale) to sub-divide each ACER
 196 record into discrete intervals and modified the time scale of the reconstructed mean annual
 197 temperature series in each interval to match the reference sequence, having normalised both
 198 sequences to remove the influence of differences in absolute values and the amplitude of
 199 changes. The adjusted age model for each ACER record was then applied to the reconstructions
 200 of MTCO, MTWA, and α from that record for subsequent analyses.

201 **2.4. Assessment of regional climate changes during Greenland D-O warming events**

202 The magnitude of climate change during the interval corresponding to each D-O warming event
 203 as registered in Greenland is calculated individually for each climate variable at each site. To
 204 avoid making an assumption about the sign of the climate change at a site, we used a third-
 205 order polynomial to fit the reconstructions during the interval from 300 years before to 600
 206 years after the official start date [corresponding to Greenland D-O warming foref](#) each event
 207 (Wolff et al., 2010; converted into AICC2012 timescale) to determine whether the change was
 208 positive or negative. We ~~then found~~[used](#) the ages corresponding to the minimum and maximum
 209 in the fitted polynomial ($t_{\min \text{ polynomial}}$, $t_{\max \text{ polynomial}}$). ~~SHowever, since~~ the smoothed polynomial
 210 may underestimate or overestimate the amplitude of change, we used the reconstructed
 211 minimum or maximum value within the period $t_{\min \text{ polynomial}} \pm 100$ years or $t_{\max \text{ polynomial}} \pm 100$
 212 years respectively (see Figure [S2S3 for illustration](#)).

213 In cases where no change was registered for all of the three climate variables, we assume that
 214 the event was not registered at the site. As a measure of the accuracy of the DTW method to
 215 identify D-O events, we compared the number of identified events with the number of D-O
 216 events that [should](#) ~~occurred~~ during the time covered by each record (Table 1). To assess
 217 whether events were missed in a particular record due to low sampling resolution, we examined
 218 the number of samples present in the 900-year interval covering the sampled D-O (i.e. 300

219 years before to 600 years after the official start date of each event), where low resolution was
 220 defined as ≤ 3 samples in this 900-year interval. Reconstructions covering intervals where a
 221 signal was not identified were not used in subsequent analyses.

222 We calculated sample-specific errors for the minimum and maximum reconstructed values.
 223 Assuming that the minimum and maximum values are independent, we used error propagation
 224 to obtain the error of the change:

$$225 \quad \sigma_{change} = \sqrt{\sigma_{min}^2 + \sigma_{max}^2}$$

226 Following Liu et al. (2022), we used a maximum likelihood method to estimate the ratio of
 227 ΔMTCO to ΔMTWA (and ratio of $\Delta\alpha$ to ΔMTWA) to take account of the errors on both
 228 variables.

229 3. Results

230 fxTWA-PLS reproduces the modern climate reasonably well (Table 2; [Figure S4.1 & 4.2](#)). The
 231 performance is best for MTCO ($R^2 = 0.75$, $\text{RMSEP} = 6.524$, slope $= 0.85$) but is also good for
 232 MTWA ($R^2 = 0.6059$, $\text{RMSEP} = 3.5868$, slope $= 0.724$) and α ($R^2 = 0.65$, $\text{RMSEP} = 0.183$,
 233 slope $= 0.71$). Assessment of the variance inflation factor scores shows that there is no problem
 234 of multicollinearity so that it is possible to reconstruct all three climate variables independently
 235 ([Supplementary Table 1 Liu et al., 2023](#)).

236 The use of dynamic time-warping made it possible to identify D-O events robustly ([Figure](#)
 237 [S5.1 ~ S5.8](#); Table 1; [Supplementary Table 42](#)). ~~Thirteen-13~~ of the 73 sites cover some part of
 238 the 50-30 ka periods but do not include D-O events. Across the remaining ~~6060~~ sites, we
 239 identified ~~285278~~ out of the ~~328348~~ individual D-O events (~~87 %80%~~) that ~~occurred-should~~
 240 ~~occur~~ during the intervals covered by the records. In the majority of cases where a D-O event
 241 should have been registered but could not be identified in an individual record (~~37 60~~-out of
 242 ~~4370~~ cases), the resolution of that part of the record was extremely poor (≤ 3 samples in the
 243 900-year interval starting 300 years before to 600 years after the official start date of the event).

244 ~~$\Delta\text{Changes in both}$~~ ΔMTCO and ΔMTWA were generally largest in the extratropics and were
 245 more muted in the tropics (Figure 3). ~~$\Delta\text{The change in}$~~ ΔMTCO was [found to be](#) significantly
 246 larger [than \$\Delta\text{MTWA}\$](#) in the northern extratropics when considered across all D-O events and

247 sites; ~~Δ the change in~~ MTCO was ~~found to be~~ larger ~~than Δ MTWA~~, but not significantly larger,
 248 in the southern extratropics; ~~Δ MTCO was found to be not correlated with Δ MTWA in the~~
 249 ~~tropics~~; ~~the changes in MTCO are not correlated with the changes in MTWA in the tropics~~
 250 (Table 3). ~~However,~~ ~~there~~ ~~was~~ a significant positive relationship between the ~~change in α~~
 251 and ~~the change in~~ MTWA in all regions (Figure 4; Table 4).

252 The spatial patterns of ~~Δ MTCO and Δ MTWA~~ ~~changes in MTCO and MTWA~~ show consistent
 253 features across multiple D-O events (Figure 5), most noticeably that the largest warming occurs
 254 in the extratropics of Eurasia, while western North America and the southern extratropics are
 255 characterised by cooling. ~~These patterns are also shown if only those reconstructions where the~~
 256 ~~change is twice that of the sample specific error are considered (Figure S6), showing that the~~
 257 ~~spatial patterns are robust to the choice of threshold. These patterns are robust when considering~~
 258 ~~only those reconstructions where the change is twice that of the sample specific error (Figure~~
 259 ~~S6).~~ The anti-phasing between the northern and southern extratropics is consistent across D-O
 260 events. Nevertheless, both the magnitude of the changes and the spatial patterns vary between
 261 the D-O events (Figure S7.13; Figure S4S7.2). ~~Changes in α~~ broadly follows the changes in
 262 temperature, with increased α in regions characterised by warming (Figure 5) but show more
 263 variability both spatially and between D-O events (Figure S7.35). This is particularly true for
 264 Europe, which is characterised by a mixed signal of drying and wetting.

265 4. Discussions and Conclusions

266 We have presented a first attempt to map the spatial patterns of quantitative changes in seasonal
 267 temperature and plant-available moisture during D-O events globally, using a consistent
 268 methodology and a single data source. These analyses show that there is an anti-phasing
 269 between changes in the northern extratropics and the southern extratropics, with warming in
 270 the north and cooling in the south. The largest and most consistent warming during D-O events
 271 occurs in Eurasia. There is a significant difference in the warming during winter and summer
 272 in the northern extratropics, resulting in an overall reduction in seasonality, but no significant
 273 difference in the ~~tropics and~~ southern extratropics. Site-based reconstructions (e.g. Denton et
 274 al., 2022; Zander et al., 2024) suggest much larger cooling in winter than summer during cold
 275 phases of the last glacial, implying enhanced seasonality compared to warm intervals, which
 276 would be consistent with our reconstructions of a reduction in seasonality during warming
 277 events in the northern extratropics. Globally, there is a positive relationship between the change

278 in temperature and plant available moisture, as indicated by α . This is consistent with more
279 qualitative interpretation of palaeo-records from specific regions, where many regions are
280 characterised by both warming and wetting (e.g. western Europe: Sánchez Goñi et al., 2008;
281 Fletcher et al., 2010; eastern Europe: Fleitmann et al., 2009; Stockehecke et al., 2016; central
282 Siberia: Grygar et al., 2006; the Great Basin USA: Denniston et al., 2007; Jiménez-Moreno et
283 al., 2010). However, according to our reconstructions, the nature of this relationship varies
284 between regions: there are some regions that are characterised by warming and wetting, others
285 are characterised by warming and drying (Figure 4; Figure 5). Previous studies have also
286 indicated drier conditions during D-O events, particularly in parts of the USA such as the
287 Pacific Northwest (Grigg and Whitlock, 2002) and Florida (Grimm et al., 2006; Jiménez-
288 Moreno et al., 2010). Although there is some consistency in the broadscale patterns of changes
289 across D-O events, the magnitude of the changes as well as the spatial patterning varies
290 between events (Figure S7.1~7.3).

291 We have used a global pollen data set for calibration of the pollen-climate relationships. The
292 use of a global data set, rather than region-specific training data, relies on the principle of
293 phylogenetic niche conservatism (Harvey and Pagel, 1991; Qian and Ricklefs 2004; Wang et
294 al., 2025), which states that traits tend to remain constant over time. This also applies to the
295 climate niche (Wiens and Graham, 2005; Wiens et al., 2010; Peterson, 2011; Crisp and Cook,
296 2012; Jiang et al., 2023) as evidenced by disjunct distributions of taxa across different
297 continents (Yin et al., 2021). Niche conservatism underpins the fact that the modern
298 distribution of specific genera can be predicted using climate-pollen relationships developed
299 from other regions (e.g. Huntley et al., 1989). The use of a global dataset for calibration makes
300 it possible to sample a large range of climates, and specifically to reconstruct climate variables
301 that might be very different from the range experienced in a region in the modern day. This is
302 particularly important when reconstructing changes in the fundamentally different climate of
303 the last glacial. Reconstructed glacial climates at some sites were indeed found to exceed the
304 climate ranges sampled for the region under modern conditions, most noticeably MTCO and
305 MTWA in the southern extratropics (Figure S8). However, the use of a global data set can
306 create issues because of inconsistencies in taxonomic resolution between regions. The
307 necessity for treating all species of *Quercus* as a single taxon, despite the fact that evergreen
308 and deciduous species may occupy distinct climate niches in some regions such as Europe, is
309 a consequence of this. However, we have shown (Supplementary Materials, Section 4) that this

310 ~~has little impact on our reconstructions – largely because the climatic distinction that would be~~
311 ~~conveyed through separating deciduous and evergreen *Quercus* is also registered by the~~
312 ~~presence of other taxa. Although the use of a global training data set for climate reconstructions~~
313 ~~has not been a common practice, it also facilitates making reconstructions for sites from regions~~
314 ~~with limited modern pollen data or where the modern samples do not capture the very different~~
315 ~~climates that might have occurred in that region during glacial times. The use of a global~~
316 ~~dataset for calibration makes it possible to sample a large range of climates. The reconstructed~~
317 ~~glacial climates were found to sometimes exceed their modern climate ranges in this region,~~
318 ~~especially for MTCO and MTWA at southern extratropics (see Figure S8). If we used a regional~~
319 ~~training, they would be limited to the regional modern climate ranges. However, the use of a~~
320 ~~global data set can create issues because of inconsistencies in taxonomic resolution between~~
321 ~~regions. The necessity for treating all species of *Quercus* as a single taxon, despite the fact that~~
322 ~~evergreen and deciduous species may occupy distinct climate niches in some regions such as~~
323 ~~Europe, is a consequence of this. Yet, as we have shown (Supplementary Materials,~~
324 ~~Figures/Tables denoted with “QR”), this has little impact on our reconstructions – largely~~
325 ~~because the climatic distinction that would be conveyed through separating deciduous and~~
326 ~~evergreen *Quercus* is also registered by the presence of other taxa, thus insensitive to the~~
327 ~~information loss of a single taxon. Although the use of a global training data set for climate~~
328 ~~reconstructions has not been a common practice, it also facilitates making reconstructions for~~
329 ~~sites from regions with limited modern pollen data or where the modern samples do not~~
330 ~~capture the very different climates that might have occurred in that region during glacial times.~~

331
332 ~~We have used a global pollen data set for calibration of the pollen-climate relationships,~~
333 ~~SMPDsv2 (Villegas-Diaz and Harrison, 2022). The use of a global data set, rather than region-~~
334 ~~specific training data, relies on the principle of phylogenetic niche conservatism (Harvey and~~
335 ~~Pagel, 1991), which states that traits tend to remain constant over time. This also applies to the~~
336 ~~climate niche (Wiens and Graham, 2005; Wiens et al., 2010; Peterson, 2011; Crisp and Cook,~~
337 ~~2012; Jiang et al., 2023) as evidenced by disjunct distributions of taxa across different~~
338 ~~continents (Yin et al., 2021). Niche conservatism underpins the fact that the modern~~
339 ~~distribution of specific genera can be predicted using climate-pollen relationships developed~~
340 ~~from other regions (e.g. Huntley et al., 1989). The use of a global data set for calibration makes~~

341 ~~it possible to sample a large range of climates, and thus makes it more likely that the~~
342 ~~reconstructions of glacial climates are realistic and not confined to the limited climate range~~
343 ~~sampled in any one region (Turner et al., 2020). Indeed, Turner et al. (2020) have shown that~~
344 ~~increasing the size of the calibration data set tends to lead to smaller reconstruction errors and~~
345 ~~more accurate estimates of taxon coefficients. Pragmatically, the use of a global data set also~~
346 ~~facilitates making reconstructions for sites from regions where there is limited modern pollen~~
347 ~~data.~~

348 These reconstructions can be used as targets for model evaluation, specifically the two transient
349 D-O experiments planned for the next phase of the Palaeoclimate Modelling Intercomparison
350 (see Malmierca-Vallet et al., 2023 for the experimental protocol). The first of these experiments
351 is a baseline simulation starting at 34 ka, a time with low obliquity, moderate MIS3 greenhouse
352 gas values, and an intermediate ice sheet configuration, which appears to be most conducive to
353 generating D-O like behaviour in climate models. The second experiment involves the addition
354 of freshwater, to examine whether this is necessary to precondition a state conducive to
355 generating D-O events. The observed anti-phasing in temperature changes between the
356 northern and southern hemispheres is a general feature of climate model experiments. Most
357 models show larger warming in winter than in summer in the northern hemisphere (e.g.
358 Flückiger et al., 2008; ~~Van Meersbeek~~[Van Meerbeeck](#) et al., 2011; Izumi et al., 2023), which
359 is also consistent with our reconstructions. Models generally show an intensification of the
360 northern hemisphere monsoons during D-O events (e.g. Menviel et al., 2020; Izumi et al, 2023),
361 but there is less consistency about changes in plant-available moisture in the extratropics. Our
362 reconstructions of α suggest an intensification of the northern hemisphere monsoons, consistent
363 with the simulations, and provide an opportunity to evaluate spatial patterns of moisture
364 changes over the extratropics. The reconstructions also indicate an increase in α across much
365 of the tropics, including northern South America, ~~West Africa and~~ southern China and Japan
366 ([Figure 5](#)). Although α is not a direct reflection of summer precipitation, these changes are
367 consistent with enhanced northern hemisphere monsoons during warming events, as shown by
368 speleothem records from the Caribbean (Warken et al, 2019) and speleothem and pollen records
369 from Asia (Wang et al., 2001; Zorzi et al., 2022; Fohlmeister et al., 2023). ~~Although there is~~
370 ~~some consistency in the broadscale patterns of changes in temperature and moisture across D-~~
371 ~~O events, the magnitude of the changes as well as the spatial patterning varies between events.~~

~~The LOVECLIM model is used as a reference to adjust the age scale in the reconstructions using MAT, but this does not preclude comparison of the reconstructed and simulated seasonal temperatures. The general spatial pattern of simulated changes in MTCO and MTWA (Figure S9.1) is consistent with the reconstructions, with largest warming in Eurasia, and cooling over most of the southern extratropical land. However, there are important differences. The reconstructions show cooling over western North America in both seasons, for example, but only in winter in the simulations. The relationship between Δ MTCO versus Δ MTWA is also different (Figure S9.2): the simulated Δ MTCO is shown to be significantly larger than Δ MTWA in the northern extratropics, but significantly smaller than Δ MTWA in the southern extratropics (Supplementary Table 3). This comparison illustrates the usefulness of the reconstructions for model evaluation and to investigate the mechanisms that may not be adequately captured by current models.~~

~~LOVECLIM model is used as a reference to adjust the age scale in the reconstructions. However, since the variable used to do the adjustment is MAT, and that the age moves synchronously for all the climate variables, we can still compare the seasonal temperatures. The general spatial pattern (Figure S9.1) is consistent with the reconstructions, with largest warming in Eurasia, and cooling in most of the southern extratropics land. However, the cooling over western North America can only be seen in MTCO but not MTWA. The seasonality is also a bit different: the scatterplot of Δ MTCO versus Δ MTWA has a different shape (Figure S9.2), and Δ MTCO is shown to be significantly larger than Δ MTWA in the northern extratropics, but significantly smaller than Δ MTWA in the southern extratropics (Supplementary Table 3). These indicate the potential of incorporating reconstructions into models to obtain a more realistic picture of the past climates.~~

Identifying D-O events in pollen records is often problematic, particularly in regions where warming (especially if accompanied by dryer conditions) leads to a reduction (or an hiatus) in sedimentation as reflected in the variable resolution of the available pollen records (e.g. Sinopoli et al., 2019; Wei et al., 2021; Camuera et al., 2022; Pini et al., 2022). The use of [dynamic time warping \(DTW: Belman and Kalaba, 1959; Burstyn et al., 2021; Alshehri et al., 2019\)](#) ~~shorter periods (Alshehri et al., 2019)~~ goes some way to improving the identification of potential D-O events ~~using dynamic time warping (Alshehri et al., 2019)~~. ~~However, it precludes the calculation of a rate of change in climate. Thus, we have focused here on the absolute magnitude of the changes during specific warming events. Thus, we were able to identify D-O events only 80% of the 348 individual D-O events that occurred during the intervals covered by the 60 records available globally.~~ It is also likely that some of the variability in the

405 reconstructed changes between different D-O events reflects imperfect identification of
406 specific events because of the comparatively modest resolution of the records. Several new
407 high-resolution records covering MIS3 have become available since the compilation of the
408 ACER database (e.g. Bird et al., 2024; Wei et al., 2021; Camuera et al., 2022; Pini et al., 2022;
409 Rowe et al., 2024; Shichi et al., 2023; Zorzi et al., 2022) and including these newer records
410 could help to improve the reliability of the global reconstructions presented here. ~~Nevertheless,
411 this first compilation of quantitative climate reconstructions through multiple D-O events
412 during MIS3 provides an opportunity for evaluation of the transient D-O simulations planned
413 as part of the next phase of the Palaeoclimate Modelling Intercomparison Project (Malmierca-
414 Vallet et al., 2023).~~

415

416

417 **Data and code availability.** All the data used are public access and cited here. The code used
418 to generate the reconstructions and figures is available at [https://github.com/ml4418/DO-
419 climate-reconstruction-paper.git](https://github.com/ml4418/DO-climate-reconstruction-paper.git)

420 **Author contributions.** ML, SPH and ICP designed the study. ML made the reconstructions
421 and produced the figures and tables. ML and SPH carried out the analyses. SPH wrote the first
422 draft of the paper and all authors contributed to the final draft.

423 **Competing Interests.** The authors declare not competing interests.

424 **Acknowledgements.** ML acknowledges support from Imperial College through the Lee
425 Family Scholarship. ICP acknowledges support from the ERC under the European Union
426 Horizon 2020 research and innovation programme (grant agreement no.: 787203 REALM).
427 SPH acknowledges fruitful discussions with colleagues from the D-O community working
428 group.

429

430 **References**

431 Adolphi, F., Bronk Ramsey, C., Erhardt, T., Edwards, R. L., Cheng, H., Turney, C. S. M.,
432 Cooper, A., Svensson, A., Rasmussen, S. O., Fischer, H., and Muscheler, R.:

- 433 Connecting the Greenland ice-core and U—/ Th timescales via cosmogenic
434 radionuclides: testing the synchronicity of Dansgaard–Oeschger events, *Clim. Past*, 14,
435 1755–1781, <https://doi.org/10.5194/cp-14-1755-2018>, 2018.
- 436 Alshehri, M., Coenen, F., and Dures, K.: Effective sub-sequence-based dynamic time warping.
437 In: Bramer, M., Petridis, M. (eds) *Artificial Intelligence XXXVI. SGAI 2019. Lecture*
438 *Notes in Computer Science*, 11927. Springer, Cham. [https://doi.org/10.1007/978-3-](https://doi.org/10.1007/978-3-030-34885-4_23)
439 [030-34885-4_23](https://doi.org/10.1007/978-3-030-34885-4_23), 2019.
- 440 Ampel, L., Bigler, C., Wohlfarth, B., Risberg, J., Lotter, A.F., and Veres, D.: Modest summer
441 temperature variability during DO cycles in western Europe, *Quat. Sci. Rev.*, 29, 1322–
442 1327, <https://doi.org/10.1016/j.quascirev.2010.03.002>, 2010.
- 443 Bauska, T. K., Marcott, S. A. and Brook, E. J.: Abrupt changes in the global carbon cycle
444 during the last glacial period, *Nat. Geosci.*, 14(2), 91–96, doi:10.1038/s41561-020-
445 00680-2, 2021.
- 446 Bellman, R., and Kalaba, R.: On adaptive control processes, *Automatic Control, IRE*
447 *Transactions*, 4, 1–9, http://ieeexplore.ieee.org/xpls/abs_all.jsp?arnumber=1104847,
448 1959.
- 449 Bird, M., Brand, M., Comley, R., Fu, X., Hadeen, X., Jacobs, Z., Rowe, C., Wurster, C., Zwart,
450 C. and Bradshaw, C.: Late Pleistocene emergence of an anthropogenic fire regime in
451 Australia’s tropical savannahs, *Nat. Geosci.*, 17, doi:10.1038/s41561-024-01388-3,
452 2024.
- 453 Burstyn, Y., Gazit, A., and Omri Dvir, O.: Hierarchical Dynamic Time Warping methodology
454 for aggregating multiple geological time series, *Comp. & Geosci.*, 150, 104704,
455 <https://doi.org/10.1016/j.cageo.2021.104704>, 2021.
- 456 Camuera, J., Ramos-Román, M.J., Jiménez-Moreno, G. *et al.*: Past 200 kyr hydroclimate
457 variability in the western Mediterranean and its connection to the African Humid
458 Periods, *Sci. Rep.*, 12, 9050, <https://doi.org/10.1038/s41598-022-12047-1>, 2022.
- 459 Corrick, E.C., Drysdale, R.N., Hellstrom, J.C., Capron, E., Rasmussen, S.O., Zhang, X.,
460 Fleitmann, D., Couchoud, I., and Wolff, E.: Synchronous timing of abrupt climate

- 461 changes during the last glacial period, *Science*, 369, 963–969,
462 <https://doi.org/10.1126/science.aay5538>, 2020.
- 463 Crisp, M. D. and Cook, L. G.: Phylogenetic niche conservatism: What are the underlying
464 evolutionary and ecological causes?, *New Phytol.*, 196(3), 681–694,
465 [doi:10.1111/j.1469-8137.2012.04298.x](https://doi.org/10.1111/j.1469-8137.2012.04298.x), 2012.
- 466 Dansgaard, W., Johnsen, S.J., Clausen, H.B., Dahl-Jensen, D., Gundestrup, N.S., Hammer,
467 C.U., Hvidberg, C.S., Steffensen, J.P., Sveinbjörnsdóttir, A.E., Jouzel, J., and Bond,
468 G.: Evidence for general instability of past climate from a 250-kyr ice-core record,
469 *Nature*, 364, 218–220, <https://doi.org/10.1038/364218a0>, 1993.
- 470 Denniston, R.F., Asmerom, Y., Polyak, V., Dorale, J.A., Carpenter, S.J., Trodick, C., Hoye,
471 B., and González, L.A.: Synchronous millennial-scale climatic changes in the Great
472 Basin and the North Atlantic during the last interglacial. *Geology* 35, 619–622, 2007.
- 473 Doblus-Reyes, F. J., Sörensson, A. A., Almazroui, M., Dosio, A., Gutowski, W. J., Haarsma,
474 R., Hamdi, R., Hewitson, B., Kwon, W.-T., Lamptey, B. L., Maraun, D., Stephenson,
475 T. S., Takayabu, I., Terray, L., Turner, A. and Zuo, Z.: Linking global to regional
476 climate change, in *Climate Change 2021 – The Physical Science Basis: Working Group
477 I Contribution to the Sixth Assessment Report of the Intergovernmental Panel on
478 Climate Change*, edited by V. Masson-Delmotte, P.Zhai, A. Pirani, S. L. Connors, C.
479 Péan, S. Berger, N. Caud, Y. Chen, L. Goldfarb, M. I. Gomis, M. Huang, K. Leitzell,
480 E.Lonnoy, J. B. R. Matthews, T. K. Maycock, T. Waterfield, O. Yelekçi, R. Yu, and B.
481 Zhou, pp. 1363–1512, Cambridge University Press, Cambridge, United Kingdom and
482 New York, NY, USA., 2021.Fleitmann, D., Cheng, H., Badertscher, S., Edwards, R.L.,
483 Mudelsee, M., Göktürk, O.M., Fankhauser, A., Pickering, R., Raible, C.C., Matter, A.,
484 Kramers, J., and Tüysüz, O.: Timing and climatic impact of Greenland interstadials
485 recorded in stalagmites from northern Turkey, *Geophys. Res. Lett.*, 36, 2009.
- 486 Fletcher, W.F., Sánchez Goñi, M.F., Allen, J.R.M., Cheddadi, R., Combourieu-Nebout, N.,
487 Huntley, B., Lawson, I., Londeix, L., Magri, D., Margari, V., Müller, U.C., Naughton,
488 F., Novenko, E., Roucoux, K., Tzedakis, P.C.: Millennial-scale variability during the
489 last glacial in vegetation records from Europe, *Quat. Sci. Rev.*, 29, 2839–2864,
490 <https://doi.org/10.1016/j.quascirev.2009.11.015>, 2010.

- 491 Flückiger, J., Knutti, R., White, J.W.C., and Renssen, H.: Modeled seasonality of glacial abrupt
492 climate events, *Clim. Dyn.*, 31, 633–645, <https://doi.org/10.1007/s00382-008-0373-y>,
493 2008.
- 494 Fohlmeister, J., Sekhon, N., Columbu, A., Vettoretti, G., Weitzel, N., Rehfeld, K., Veiga-Pires,
495 C., Ben-Yami, M., Marwan, N. and Boers, N.: Global reorganization of atmospheric
496 circulation during Dansgaard–Oeschger cycles, *Proc. Natl. Acad. Sci.*, 120(36),
497 e2302283120, doi:10.1073/pnas.2302283120, 2023.
- 498 Grigg, L.D., and Whitlock, C.: Patterns and causes of millennial-scale climate change in the
499 Pacific Northwest during Marine Isotope Stages 2 and 3, *Quat. Sci. Rev.*, 21, 2067-
500 2083, 2002.
- 501 Grimm, E.C., Watts, W.A., Jacobson, G.L., Hansen, B.C.S., Almquist, H., and Dieffenbacher-
502 Krall, A.C.: Evidence for warm wet Heinrich events in Florida, *Quat. Sci. Rev.*, 25,
503 2197-2211, 2006.
- 504 Grygar, T., Kadlec, J., Pruner, P., Swann, G., Bezdicka, P., Hradil, D., Lang, K., Novotna, K.,
505 and Oberhänsli, H.: Paleoenvironmental record in Lake Baikal sediments:
506 environmental changes in the last 160 ky, *Palaeogeogr. Palaeoclimatol. Palaeoecol.*,
507 237, 240-254, 2006.
- 508 Guiot, J., de Beaulieu, J. L., Cheddadi, R., David, F., Ponel, P., and Reille, M.: The climate in
509 Western Europe during the last Glacial/Interglacial cycle derived from pollen and insect
510 remains, *Palaeogeogr., Palaeoclimatol., Palaeoecol.*, 103, 73–93,
511 [https://doi.org/10.1016/0031-0182\(93\)90053-L](https://doi.org/10.1016/0031-0182(93)90053-L), 1993.
- 512 Jiménez-Moreno, G., Anderson, R.S., Desprat, S., Grigg, L.D., Grimm, E.C., Heusser, L.E.,
513 Jacobs, B.F., López-Martínez, C., Whitlock, C.L., and Willard, D.A.: Millennial-scale
514 variability during the last glacial in vegetation records from North America, *Quat. Sci.*
515 *Rev.*, 29, 2865-2881, <https://doi.org/10.1016/j.quascirev.2009.12.013>, 2010.
- 516 Harrison, S.P., and Sánchez Goñi, M.F.: Global patterns of vegetation response to millennial-
517 scale variability during the last glacial: A synthesis. *Quat. Sci. Rev.*, 29, 2957-2980,
518 2010.

- 519 [Harrison, S.P., Bartlein, P.J., Cruz-Silva, E., Haas, O., Jackson, S.T., Kaushal, N., Liu, M.,](#)
520 [Magri, D., Robson, D., Vettoretti, G., Prentice, I.C.: Palaeoclimate perspectives on](#)
521 [contemporary climate change, *Ann. Rev. Environ. Resour.*, 50, 2025.](#)
- 522 Harvey, P. H. and Pagel, M. D.: The comparative method in evolutionary biology, Oxford
523 University Press., 1991.
- 524 Huber, C., Leuenberger, M., Spahni, R., Flückiger, J., Schwander, J., Stocker, T.F., Johnsen,
525 S., Landais, A., and Jouzel, J.: Isotope calibrated Greenland temperature record over
526 Marine Iso-tope Stage 3 and its relation to CH₄, *Earth Planet. Sci. Lett.*, 243, 504–519,
527 2006.
- 528 Huntley, B., Bartlein, P. J. and Prentice, I. C.: Climatic control of the distribution and
529 abundance of Beech (*Fagus L.*) in Europe and North America, *J. Biogeogr.*, 16(6), 551–
530 560, doi:10.2307/2845210, 1989.
- 531 Huntley, B., Watts, W.A., Allen, J.R.M., Zolitschka, B.: Palaeoclimate, chronology and
532 vegetation history of the Weichselian Lateglacial: comparative analysis of data from
533 three cores at Lago Grande di Monticchio, southern Italy, *Quat. Sci. Rev.*, 18: 945-960,
534 [https://doi.org/10.1016/S0277-3791\(99\)00007-4](https://doi.org/10.1016/S0277-3791(99)00007-4), 1999.
- 535 IPCC: Climate change 2022: Impacts, adaptation and vulnerability. Contribution of working
536 group II to the sixth assessment report of the Intergovernmental Panel on Climate
537 Change, edited by H.-O. Pörtner, D. C. Roberts, M. Tignor, E. S. Poloczanska, K.
538 Mintenbeck, A. Alegria, M. Craig, S. Langsdorf, S. Löschke, V. Möller, A. Okem, and
539 B. Rama, Cambridge University Press, Cambridge University Press, Cambridge, UK
540 and New York, NY, USA., 2022.
- 541 Jiang, K., Wang, Q., Dimitrov, D., Luo, A., Xu, X., Su, X., Liu, Y., Li, Y., Li, Y. and Wang, Z.:
542 Evolutionary history and global angiosperm species richness–climate relationships,
543 *Glob. Ecol. Biogeogr.*, 32(7), 1059–1072, doi:10.1111/geb.13687, 2023.
- 544 Kindler, P., Guillevic, M., Baumgartner, M., Schwander, J., Landais, A., and Leuenberger, M.:
545 Temperature reconstruction from 10 to 120 kyr b2k from the NGRIP ice core, *Clim.*
546 *Past*, 10, 887–902, <https://doi.org/10.5194/cp-10-887-2014>, 2014.

- 547 Lee, J.-Y., Marotzke, J., Bala, G., Cao, L., Corti, S., Dunne, J. P., Engelbrecht, F., Fischer, E.,
548 Fyfe, J. C., Jones, C., Maycock, A., Mutemi, J., Ndiaye, O., Panickal, S. and Zhou, T.:
549 Future global climate: Scenario-based projections and near-term information, in
550 Climate change 2021: The physical science basis. Contribution of working group I to
551 the sixth assessment report of the Intergovernmental Panel on Climate Change, edited
552 by V. Masson-Delmotte, P. Zhai, A. Pirani, S. L. Connors, C. Péan, S. Berger, N. Caud,
553 Y. Chen, L. Goldfarb, M. I. Gomis, M. Huang, K. Leitzell, E. Lonnoy, J. B. R.
554 Matthews, T. K. Maycock, T. Waterfield, O. Yelekçi, R. Yu, and B. Zhou, pp. 553–672,
555 Cambridge University Press, Cambridge, United Kingdom and New York, NY, USA.,
556 2021.
- 557 Liu, M., Prentice, I.C., ter Braak, C.J.F, and Harrison, S.P.: An improved statistical approach
558 for reconstructing past climates from biotic assemblages, *Proc. Royal Soc., Math. A*,
559 476, 20200346, 20200346, <https://doi.org/10.1098/rspa.2020.0346>, 2020.
- 560 Liu, M., Shen, Y., González-Sampériz, P., Gil-Romera, G., ter Braak, C.J.F. Prentice, I.C., and
561 Harrison, S.P.: Holocene climates of the Iberian Peninsula, *Clim. Past* 19, 803-834,
562 <https://doi.org/10.5194/cp-19-803-2023>, 2023.
- 563 Malmierca-Vallet, I., Sime, L.C., and the D–O community members: Dansgaard–Oeschger
564 events in climate models: review and baseline Marine Isotope Stage 3 (MIS3) protocol,
565 *Clim. Past*, 19, 915–942, <https://doi.org/10.5194/cp-19-915-2023>, 2023.
- 566 Meniel, L., Timmermann, A., Friedrich, T., and England, M. H.: Hindcasting the continuum
567 of Dansgaard–Oeschger variability: mechanisms, patterns and timing, *Clim. Past* 10,
568 63–77, 2014.
- 569 Meniel, L.C., Skinner, L.C., Tarasov, L., and Tzedakis, P.C.: An ice–climate oscillatory
570 framework for Dansgaard–Oeschger cycles, *Nat. Rev. Earth Environ.*, 1, 677–693,
571 <https://doi.org/10.1038/s43017-020-00106-y>, 2020.
- 572 Peterson, A. T.: Ecological niche conservatism: A time-structured review of evidence, *J.*
573 *Biogeogr.*, 38(5), 817–827, doi:10.1111/j.1365-2699.2010.02456.x, 2011.
- 574 Pini, R., Furlanetto, G., Vallé, F., Badino, F., Wick, L., Anselmetti, F.S., Bertuletti, P., Fusi, N.,
575 Morlock, M.A., Delmonte, B., Harrison, S.P., Maggi, V., Ravazzi, C.: Linking North

- 576 Atlantic and Alpine Last Glacial Maximum climates via a high-resolution pollen-based
577 subarctic forest steppe record, *Quat. Sci. Rev.*, 294, 107759,
578 <https://doi.org/10.1016/j.quascirev.2022.107759>, 2022.
- 579 [Prentice, I. C., Cleator, S. F., Huang, Y. H., Harrison, S. P. and Roulstone, I.: Reconstructing](#)
580 [ice-age palaeoclimates: Quantifying low-CO₂ effects on plants, *Glob. Planet. Change*,](#)
581 [149, 166–176, doi:<https://doi.org/10.1016/j.gloplacha.2016.12.012>, 2017.](#)
- 582 Prentice, I. C., Villegas-Diaz, R. and Harrison, S. P.: Accounting for atmospheric carbon
583 dioxide variations in pollen-based reconstruction of past hydroclimates, *Glob. Planet.*
584 *Change*, 211, 103790, doi:10.1016/j.gloplacha.2022.103790, 2022.
- 585 Prud'homme, C., Fischer, P., Jöris, O., Gromov, S., Vinnepand, M., Hatté, C., Vonhof, H.,
586 Moine, O., Vött, A., and Fitzsimmons, K. E.: Millennial-timescale quantitative
587 estimates of climate dynamics in central Europe from earthworm calcite granules in
588 loess deposits, *Commun. Earth Environ.*, 3, 1–14, [https://doi.org/10.1038/s43247-022-](https://doi.org/10.1038/s43247-022-00595-3)
589 [00595-3](https://doi.org/10.1038/s43247-022-00595-3), 2022.
- 590 [Qian, H. and Ricklefs, R. E.: Geographical distribution and ecological conservatism of disjunct](#)
591 [genera of vascular plants in eastern Asia and eastern North America, *J. Ecol.*, 92\(2\),](#)
592 [253–265, doi:<https://doi.org/10.1111/j.0022-0477.2004.00868.x>, 2004.](#)
- 593 Rowe, C., Brand, M., Wurster, C. M. and Bird, M. I.: Vegetation changes through stadial and
594 interstadial stages of MIS 4 and MIS 3 based on a palynological analysis of the
595 Girraween Lagoon sediments of Darwin, Australia, *Palaeogeogr. Palaeoclimatol.*
596 *Palaeoecol.*, 642, 112150, doi:10.1016/j.palaeo.2024.112150, 2024.
- 597 Sánchez Goñi, M., Cacho, I., Turon, J., Guiot, J., Sierro, F., Peypouquet, J., Grimalt, J. and
598 Shackleton, N.: Synchronicity between marine and terrestrial responses to millennial
599 scale climatic variability during the last glacial period in the Mediterranean region,
600 *Clim. Dyn.*, 19(1), 95–105, doi:10.1007/s00382-001-0212-x, 2002.
- 601 Sánchez Goñi, M.F., and Harrison, S.P.: Millennial-scale climate variability and vegetation
602 changes during the Last Glacial: Concepts and terminology, *Quat. Sci. Rev.*, 29, 2823–
603 2827, 2010.

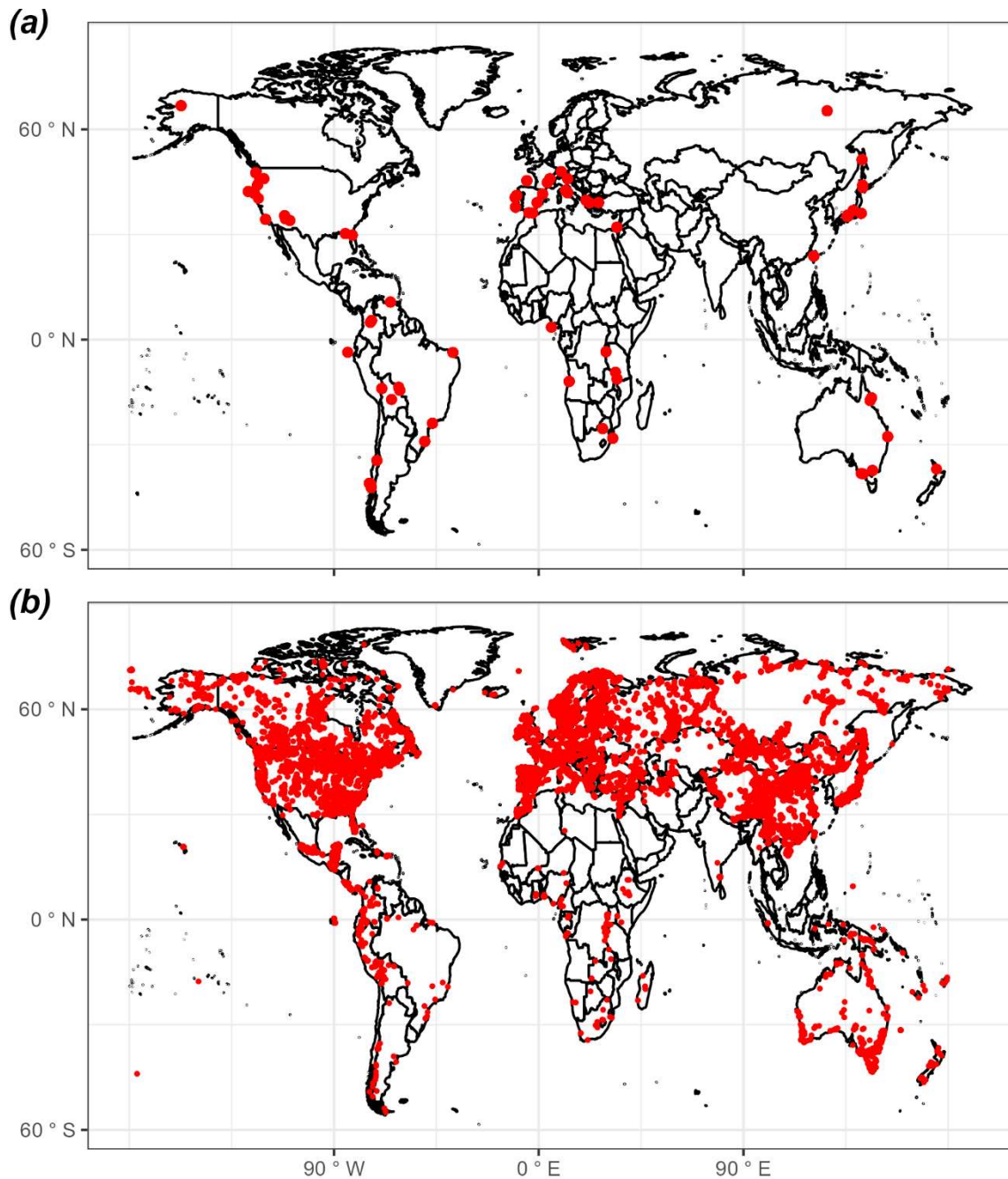
- 604 Sánchez Goñi, M.F., Desprat, S., Danialu, A.-L., Bassinot, F., Polanco-Martínez, J.M., Harrison,
605 S.P., Allen, J.R.P., Anderson, R.S., Behling, H., Bonnefille, R., Burjachs, F., Carrión,
606 J.S., Cheddadi, R., Clark, J.S., Combourieu-Nebout, N., Courtney-Mustaphi, C.,
607 Debusk, G.H., Dupont, L.M., Finch, J., Fletcher, W.J., Giardini, M., González, C.,
608 Gosling, W.D., Grigg, L.D., Grimm, E.C., Hayashi, R., Helmens, K., Heusser, L.E.,
609 Hill, T., Hope, G., Huntley, B., Igarashi, Y., Irino, T., Jacobs, B.F., Jiménez-Moreno, G.,
610 Kawai, S., Kershaw, P., Kumon, F., Lawson, I., Ledru, M.-P., Lézine, A.-M., Liew, P.-
611 M., Magri, D., Marchant, R., Margari, V., Mayle, F., McKenzie, M., Moss, P., Müller,
612 S., Müller, U.C., Naughton, F., Newnham, R.M., Oba, T., Pérez-Obiol, R., Pini, R.,
613 Ravazzi, C., Roucoux, K.H., Rucina, S., Scott, L., Takahara, H., Tzedakis, P.C., Urrego,
614 D.H., Van Geel, B., Valencia, B.G., Vandergoes, M.J., Vincens, A., Whitlock, C.L.,
615 Willard, D. A., and Yamamoto, M.: The ACER pollen and charcoal database: a global
616 resource to document vegetation and fire response to abrupt climate changes of the last
617 glacial period, *Earth Syst. Sci. Data* 9: 679-695, 2017.
- 618 Shichi, K., Goebel, T., Izuho, M. and Kashiwaya, K.: Climate amelioration, abrupt vegetation
619 recovery, and the dispersal of *Homo sapiens* in Baikal Siberia, *Sci. Adv.*, 9(38),
620 eadi0189, doi:10.1126/sciadv.adi0189, 2024.
- 621 Sinopoli, G., Peyron, O., Masi, A., Holtvoeth, J., Francke, A., Wagner, B., and Sadori, L.:
622 Pollen-based temperature and precipitation changes in the Ohrid Basin (western
623 Balkans) between 160 and 70 ka, *Clim. Past*, 15, 53–71, [https://doi.org/10.5194/cp-15-](https://doi.org/10.5194/cp-15-53-2019)
624 53-2019, 2019.
- 625 Stockhecke, M., Timmermann, A., Kipfer, R., Haug, G.H., Kwiecien, O., Friedrich, T.,
626 Menviel, L., Litt, T., Pickarski, N., and Anselmetti, F.S.: Millennial to orbital-scale
627 variations of drought intensity in the Eastern Mediterranean, *Quat. Sci. Rev.*, 133, 77-
628 95, 2016.
- 629 Turner, M. G., Wei, D., Prentice, I. C. and Harrison, S. P.: The impact of methodological
630 decisions on climate reconstructions using WA-PLS, *Quat. Res.*, 99, 341–356,
631 doi:10.1017/qua.2020.44, 2021.
- 632 Újvári, G., Bernasconi, S. M., Stevens, T., Kele, S., Páll-Gergely, B., Surányi, G., and Demény,
633 A.: Stadial-~~i~~nterstadial ~~t~~emperature and ~~a~~ridity ~~y~~variations in ~~e~~East ~~c~~entral

- 634 Europe pPreceding the Last Glacial Maximum, *Paleoceanog. Paleoclim.*, 36,
635 e2020PA004170, <https://doi.org/10.1029/2020PA004170>, 2021.
- 636 Van Meerbeeck, C.J., Renssen, H., Roche, D.M., Wohlfarth, B., Bohncke, S.J.P., Bos, J.A.A.,
637 Engels, S., Helmens, K.F., Sánchez-Goñi, M.F., Svensson, A., and Vandenberghe, J.:
638 The nature of MIS 3 stadial-interstadial transitions in Europe: New insights from
639 model-data comparisons, *Quat. Sci. Rev.*, 30, 3618–3637,
640 <https://doi.org/10.1016/j.quascirev.2011.08.002>, 2011.
- 641 ~~Villegas-Díaz, R., and Harrison, S.P.: The SPECIAL Modern Pollen Data Set for Climate~~
642 ~~Reconstructions, version 2 (SMPDSv2). University of Reading.~~
643 ~~Dataset. <https://doi.org/10.17864/1947.000389>, 2022.~~
- 644 Voelker, A.H.: Global distribution of centennial-scale records for Marine Isotope Stage (MIS)
645 3: a database, *Quat. Sci. Rev.*, 21, 1185–1212, 2002.
- 646 Wang, Y. J., Cheng, H., Edwards, R. L., An, Z. S., Wu, J. Y., Shen, C.-C. and Dorale, J. A.: A
647 high-resolution absolute-dated Late Pleistocene monsoon record from Hulu Cave,
648 China, *Science* (80-.), 294(5550), 2345–2348, doi:10.1126/science.1064618, 2001.
- 649 [Wang, C., Wang, M., Zhu, S., Wu, X., Yang, S., Yan, Y. and Wen, Y.: Multiple ecological](#)
650 [niche modeling reveals niche conservatism and divergence in East Asian Yew \(*Taxus*\).](#)
651 [Plants, 14\(7\), doi:10.3390/plants14071094, 2025.](#)
- 652 Warken, S. F., Scholz, D., Spötl, C., Jochum, K. P., Pajón, J. M., Bahr, A. and Mangini, A.:
653 Caribbean hydroclimate and vegetation history across the last glacial period, *Quat. Sci.*
654 *Rev.*, 218, 75–90, doi:10.1016/j.quascirev.2019.06.019, 2019.
- 655 Wei, D., González-Sampériz, P., Gil-Romera, G., Harrison, S.P., and Prentice, I.C.: Seasonal
656 temperature and moisture changes in interior semi-arid Spain from the last interglacial
657 to the Late Holocene, *Quat. Res.*, 101, 143–155, <https://doi.org/10.1017/qua.2020.108>,
658 2021.
- 659 Wiens, J. and Graham, C.: Niche conservatism: Integrating evolution, ecology, and
660 conservation biology, *Annu. Rev. Ecol. Evol. Syst.*, 36, 519–539,
661 doi:10.1146/annurev.ecolsys.36.102803.095431, 2005.

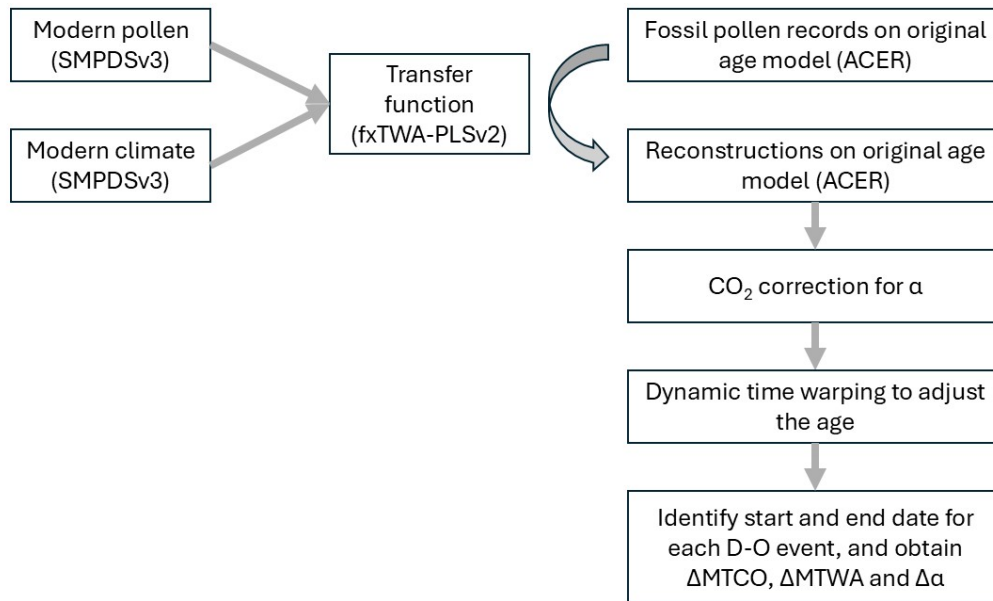
- 662 Wolff, E. W., Chappellaz, J., Blunier, T., Rasmussen, S. O. and Svensson, A.: Millennial-scale
663 variability during the last glacial: The ice core record, *Quat. Sci. Rev.*, 29(21), 2828–
664 2838, doi:10.1016/j.quascirev.2009.10.013, 2010.
- 665 Yin, X., Jarvie, S., Guo, W.-Y., Deng, T., Mao, L., Zhang, M., Chu, C., Qian, H., Svenning, J.-
666 C. and He, F.: Niche overlap and divergence times support niche conservatism in
667 eastern Asia–eastern North America disjunct plants, *Glob. Ecol. Biogeogr.*, 30(10),
668 1990–2003, doi:10.1111/geb.13360, 2021.
- 669 Zander, P. D., Böhl, D., Sirocko, F., Auderset, A., Haug, G. H. and Martínez-García, A.:
670 Reconstruction of warm-season temperatures in central Europe during the past 60 000
671 years from lacustrine branched glycerol dialkyl glycerol tetraethers (brGDGTs), *Clim.*
672 *Past*, 20(4), 841–864, doi:10.5194/cp-20-841-2024, 2024.
- 673 Zorzi, C., Desprat, S., Clément, C., Thirumalai, K., Oliviera, D., Anupama, K., Prasad, S. and
674 Martinez, P.: When eastern India oscillated between desert versus savannah-dominated
675 vegetation, *Geophys. Res. Lett.*, 49(16), e2022GL099417,
676 doi:10.1029/2022GL099417, 2022.
- 677

678 **Figures and Tables**

679 Figure 1: Map showing the locations of sites (a) from the Abrupt Climate Changes and
680 Environmental Responses (ACER) database covering the interval between 50 ka and 30 ka
681 used for the reconstructions and (b) sites in version 3 of the SPECIAL Modern Pollen Dataset
682 (SMPDSv3) used to derive the transfer functions for these climate reconstructions.



685 Figure 2: Flow chart showing the reconstruction methodology.



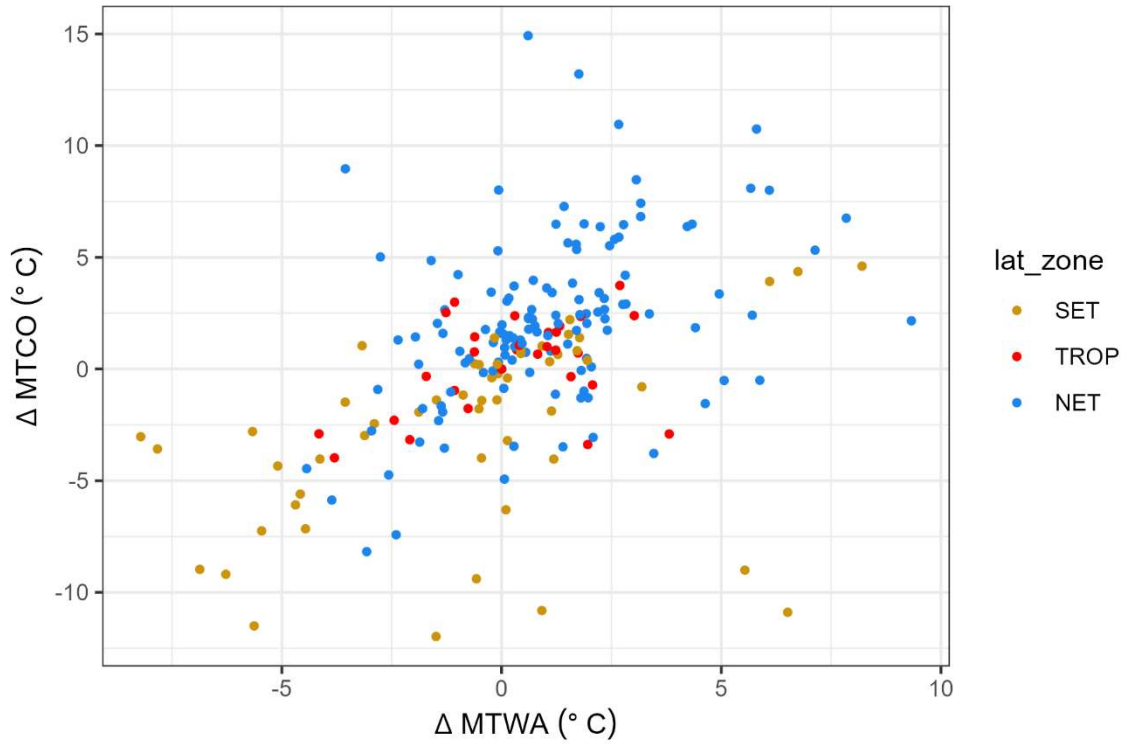
686

687

688

689

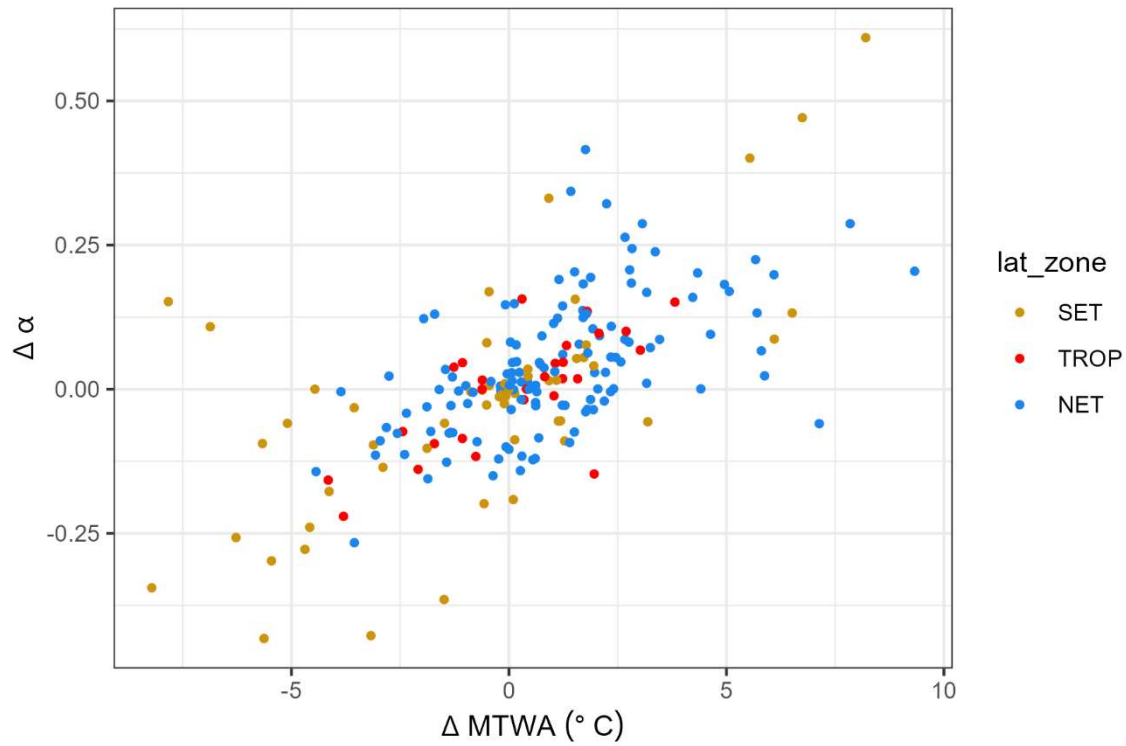
690 Figure 3: Scatter plot of the change in mean temperature of the coldest month (ΔMTCO) versus
691 the change in mean temperature of the warmest month (ΔMTWA) during individual
692 Dansgaard-Oeschger (D-O) events at individual sites. The points are colour-coded to indicate
693 whether the sites are from the northern extratropics (NET, north of 23.5°N), the tropics (TROP,
694 between 23.5°N and 23.5°S) or southern extratropics (SET, south of 23.5°S).



695

696

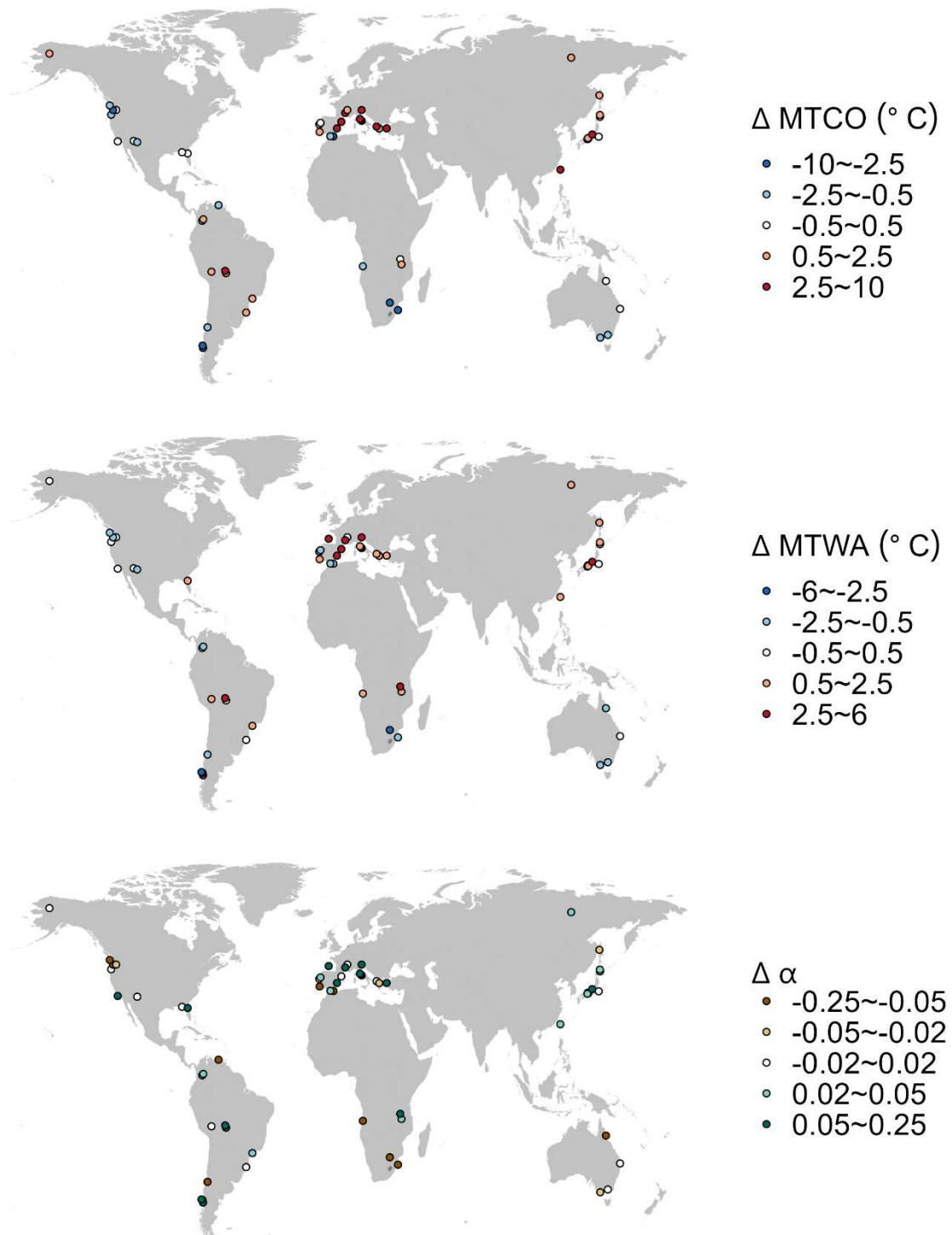
697 Figure 4: Scatter plot of the change in plant-available moisture ($\Delta\alpha$) versus the change in mean
698 temperature of the warmest month (ΔMTWA) during individual Dansgaard-Oeschger (D-O)
699 events at individual sites. The points are colour-coded to indicate whether the sites are from
700 the northern extratropics (NET, north of 23.5°N), the tropics (TROP, between 23.5°N and
701 23.5°S) or southern extratropics (SET, south of 23.5°S).



702

703

704 Figure 5: Maps showing the median change of site-based reconstructions for Dansgaard-
 705 Oeschger (D-O) events 5~12.



706

707

708 Table 1: Details of the sites from the Abrupt Climate Changes and Environmental Responses
 709 (ACER) database (Sánchez Goñi et al., 2017) covering the interval between 50 ka and 30 ka
 710 used for the climate reconstructions. n_{due} is the number of D-O events that should be found
 711 based on the time interval covered by the record. n_{miss} is the number of D-O events that were
 712 not identified. n_{low} is the number of D-O events missed because of low resolution of part of the
 713 record. Some of the 73 sites (indicated by NA in n_{due} , n_{miss} and n_{low}) provide records for parts
 714 of the 50-30ka interval but not for the intervals of the D-O events. Reconstructions based on
 715 samples where the D-O signal was not identified were not used in subsequent analyses. The
 716 full citations for each site are given in Supplementary Materials.

Site name	Latitude	Longitude	Elevation (m)	Site type	Reference(s)	n_{due}	n_{miss}	n_{low}
Abric Romani	41.53	1.68	350	TERR	Burjachs & Julià (1994)	2	0	0
Azzano Decimo	45.8833	12.7165	10	TERR	Pini et al. (2009)	6	2	2
Caledonia Fen	-37.3333	146.7333	1280	TERR	Kershaw et al. (2007b)	8	0	0
Cambara do Sul	-29.05	-50.1	1040	TERR	Behling et al. (2004)	7	0	0
Camel Lake	30.26	-85.01	20	TERR	Watts et al. (1992)	2	1	1
Carp Lake	45.91	-120.88	720	TERR	Whitlock and Bartlein (1997); Whitlock et al. (2000)	8	1	1
Colônia	-23.87	-46.71	900	TERR	Ledru et al. (2009)	7	2	2
Core Trident 163 31B	-3.61	-83.96	-3210	MARI	Heusser and Shackleton (1994)	NA	NA	NA
Fargher Lake	45.88	-122.58	200	TERR	Grigg and Whitlock (2002)	8	2	1
Fundo Nueva	-41.28	-73.83	66	TERR	Heusser et al. (2000)	6	1	0
Fuquene	5.45	-73.46	2540	TERR	van Geel and van der Hammen (1973); Mommersteeg (1998)	7	3	3
Füramoos	47.98	9.88	662	TERR	Müller et al. (2003)	NA	NA	NA
GeoB3104	-3.67	-37.72	-767	MARI	Behling et al. (2000)	NA	NA	NA
Hay Lake	34	-109.425	2780	TERR	Jacobs (1985)	5	3	3
Ioannina	39.75	20.85	470	TERR	Tzedakis et al. (2002); Tzedakis et al. (2004)	8	1	0
Joe Lake	66.76667	-157.217	183	TERR	Anderson (1988); Anderson et al. (1994)	7	3	3
Kalaloch	47.6053	-124.371	19	TERR	Heusser (1972)	8	1	0
Kamiyoshi Basin (KY01)	35.102	135.586	335	TERR	Takahara et al. (2000);; Takahara et al. (2007); Hayashi et al. (2009)	2	0	0
Kashiru Bog	-3.47	29.57	2240	TERR	Bonnefille & Riollet (1988); Bonnefille et al. (1992)	2	2	2
Kenbuchi Basin	44.05	142.383	135	TERR	Igarashi et al. (1993); Igarashi (1996)	3	0	0
Khoe	51.341	142.14	15	TERR	Igarashi et al. (2002)	6	2	2
Kohuora	-36.95	174.8667	5	TERR	Newnham et al. (2007)	NA	NA	NA
Kurota Lowland	35.517	135.879	20	TERR	Takahara & Kitagawa (2000)	3	0	0
KW31	3.52	5.57	-1181	MARI	Lézine & Cazet (2005);	NA	NA	NA

					Lézine et al. (2005)			
La Laguna	4.92	-74.03	2900	TERR	Helmens et al., 1(1996)	2	0	0
Lac du Bouchet	44.83	3.82	1200	TERR	Reille and de Beaulieu (1990)	8	0	0
Lagaccione	42.57	11.8	355	TERR	Magri (1999); Magri (2008)	7	0	0
Laguna Bella Vista	-13.6167	-61.55	600	TERR	Burbridge et al. (2004)	2	0	0
Laguna Chaplin	-14.4667	-61.0667	600	TERR	Burbridge et al. (2004)	3	0	0
Lake Billyakh	65.2833	126.7833	340	TERR	Müller et al. (2010)	4	0	0
Lake Biwa (BIW95-4)	35.245	136.054	84	TERR	Takemura et al. (2000); Hayashida et al. (2007); Hayashi et al. (2010)	3	0	0
Lake Consuelo (CON1)	-13.95	-68.991	1360	TERR	Urrego et al. (2005); Urrego et al. (2010)	7	0	0
Lake Malawi	-11.22	34.42	470	TERR	DeBusk (1998)	6	1	1
Lake Masoko	-9.33	33.75	840	TERR	Vincens et al. (2007)	2	0	0
Lake Nojiri	36.831	138.216	657	TERR	Kumon et al. (2009)	8	0	0
Lake Tulane	29.83	-81.95	36	TERR	Grimm et al. (1993); Grimm et al. (2006)	8	2	2
Lake Wangoom LW87 core	-38.35	142.6	100	TERR	Harle et al. (2002)	7	1	1
Lake Xinias	39.05	22.27	500	TERR	Bottema (1979)	8	3	3
Les Echets G	45.9	4.93	267	TERR	de Beaulieu & Reille (1984)	8	1	0
Little Lake	44.16	-123.58	217	TERR	Grigg et al. (2001)	5	0	0
Lynchs Crater	-17.3667	145.7	760	TERR	Kershaw et al. (2007a)	8	1	1
MD01-2421	36.02	141.77	-2224	MARI	Igarashi & Oba (2006); Oba et al. (2006); Aoki et al. (2008)	8	0	0
MD03-2622 Cariaco Basin	10.7061	-65.1691	-877	MARI	González et al. (2008); González and Dupont (2009)	3	0	0
MD04-2845	45.35	-5.22	-4100	MARI	Sánchez Goñi et al. (2008); Daniau et al. (2009)	2	0	0
MD84-629	32.07	34.35	-745	MARI	Cheddadi & Rossignol-Strick (1995)	NA	NA	NA
MD95-2039	40.58	-10.35	-3381	MARI	Roucoux et al. (2001); Roucoux et al. (2005)	5	0	0
MD95-2042	37.8	-10.17	-3148	MARI	Sánchez Goñi et al. (1999); Sánchez Goñi et al. (2000); Daniau et al. (2007); Sánchez Goñi et al. (2008); (Sánchez Goñi et al. (2009)	6	0	0
MD95-2043	36.14	-2.621	-1841	MARI	Sánchez Goñi et al. (2002); Fletcher and Sánchez Goñi (2008)	4	0	0
MD99-2331	41.15	-9.68	-2110	MARI	Sánchez Goñi et al. (2005); Naughton et al. (2007); Sánchez Goñi et al. (2008); Naughton et al. (2009)	5	0	0
Megali Limni	39.1025	26.3208	323	TERR	Margari et al. (2007); Margari et al. (2009)	6	0	0
Mfabeni Peatland	-28.1487	32.51867	11	TERR	Finch & Hill (2008)	5	1	0

Nakafurano	43.367	142.433	173	TERR	Igarashi et al. (1993)	2	0	0
Native Companion Lagoon	-27.68	153.41	20	TERR	Petherick et al. (2008a); Petherick et al. (2008b)	6	0	0
Navarrés	39.1	-0.68	225	TERR	Carrión & van Geel (1999)	3	0	0
ODP 1233 C	-41	-74.45	-838	MARI	Lamy et al. (2004); Heusser et al. (2006)	6	0	0
ODP 820	-16.63	146.3	-280	MARI	Moss & Kershaw (2000); Moss & Kershaw (2007)	NA	NA	NA
ODP site 976	36.2	-4.3	-1108	MARI	Nebout et al. (2002); Masson-Delmotte et al. (2005)	7	0	0
ODP1019	41.66	-124.91	989	MARI	Mix et al. (1999); Pisias et al. (2001)	NA	NA	NA
ODP1078C	-11.92	13.4	-426	MARI	Dupont & Behling (2006); Dupont et al. (2008)	8	0	0
ODP893A	34.28	-120.03	-577	MARI	Heusser (1998); Heusser (2000)	6	0	0
Potato Lake	34.45	-111.33	2222	TERR	Anderson (1993)	4	3	3
Rice Lake (Rice Lake 81)	40.3	-123.22	1100	TERR	L. Heusser, unpublished data	NA	NA	NA
Siberia	-17.09	-64.72	2920	TERR	Mourguiart & Ledru (2003)	1	1	1
Stracciaccappa	42.13	12.32	220	TERR	Giardini (2007)	5	1	1
Tagua Tagua	-34.5	-71.16	200	TERR	Heusser (1990)	6	0	0
Taiquemo	-42.17	-73.6	170	TERR	Heusser et al. (1999); Heusser and Heusser (2006)	8	0	0
Toushe Basin	23.82	120.88	650	TERR	Liew et al. (2006)	8	1	1
Tswaing Crater	-25.4	28.08	1100	TERR	Partridge et al. (1997); Scott et al. (2008); L. Scott, unpublished data;	6	1	1
Tyrrendara Swamp	-38.1986	141.7626	13	TERR	Builth et al. (2008)	NA	NA	NA
Valle di Castiglione	41.9	12.76	44	TERR	Alessio et al. (1986); Follieri et al. (1988); Follieri et al. (1989); Narcisi et al. (1992); Narcisi (1999); Magri & Tzedakis (2000); Magri (2008)	7	2	2
W8709-13 PC	42.11	-125.75	-2712	MARI	Pisias et al. (2001)	NA	NA	NA
W8709-8 PC	42.26	-127.68	-3111	MARI	Heusser (1998); Lyle et al. (1992)	NA	NA	NA
Walker Lake	35.38	-111.71	2500	TERR	Berry et al. (1982); Adam et al. (1985); Hevly (1985)	NA	NA	NA

717

718

719 Table 2: Leave-out cross-validation (with geographically and climatically close sites removed)
 720 using fxTWA-PLSv2 for mean temperature of the coldest month (MTCO), mean temperature
 721 of the warmest month (MTWA) and plant-available water (α) with P-splines smoothed fx
 722 estimation and bins of 0.02, 0.02 and 0.002, respectively. n is the number of components where
 723 the last significant number of components is indicated in **bold** (using criteria of $p \leq 0.01$).
 724 Avg.bias is the average bias; RMSEP is the root-mean-square error of prediction;
 725 and Δ RMSEP is the per cent change of RMSEP, which is $100 \times$
 726 $(\text{RMSEP}_n - \text{RMSEP}_{n-1})/\text{RMSEP}_{n-1}$; when $n = 1$, RMSEP_0 is the RMSEP of the null
 727 model. p assesses whether using the current number of components is significantly different
 728 from using one component less. The degree of overall compression is assessed by linear
 729 regression of the cross-validated reconstructions on to the climate variable; b_1 and $b_{1.se}$ are the
 730 slope and the standard error of the slope, respectively. The closer the slope (b_1) is to 1, the less
 731 the compression.

	n	R^2	Avg.bias	RMSEP	Δ RMSEP	p	b_1	$b_{1.se}$
MTCO (°C)	1	0.72	-1.15	6.84	-45.20	0.001	0.83	0.00
	2	0.74	-1.24	6.68	-2.38	0.001	0.84	0.00
	3	0.75	-1.11	6.52	-2.37	0.001	0.85	0.00
	4	0.75	-1.12	6.54	0.33	0.983	0.85	0.00
	5	0.75	-1.14	6.52	-0.29	0.001	0.85	0.00
MTWA (°C)	1	0.50	-0.29	4.00	-27.76	0.001	0.61	0.00
	2	0.60	-0.20	3.62	-9.42	0.001	0.71	0.00
	3	0.60	-0.23	3.58	-1.11	0.001	0.72	0.00
	4	0.60	-0.23	3.58	0.01	0.525	0.71	0.00
	5	0.60	-0.24	3.58	-0.14	0.090	0.71	0.00
α	1	0.61	-0.021	0.191	-37.32	0.001	0.66	0.00
	2	0.62	-0.023	0.189	-0.61	0.001	0.67	0.00
	3	0.63	-0.022	0.187	-1.18	0.001	0.68	0.00
	4	0.64	-0.021	0.184	-1.46	0.001	0.70	0.00
	5	0.64	-0.020	0.184	-0.12	0.002	0.70	0.00
	6	0.64	-0.020	0.184	-0.25	0.001	0.70	0.00
	7	0.65	-0.019	0.183	-0.26	0.001	0.71	0.00
	8	0.65	-0.019	0.183	-0.03	0.255	0.71	0.00
	9	0.65	-0.019	0.183	-0.05	0.121	0.71	0.00
	10	0.65	-0.019	0.183	-0.04	0.130	0.71	0.00

732

733

734 Table 3: Maximum likelihood estimates of the relationship between the change in mean
 735 temperature of the coldest month (ΔMTCO) and the change in mean temperature of the
 736 warmest month (ΔMTWA) by latitudinal bands for the northern extratropics (NET, north of
 737 23.5°N), tropics (TROP, between 23.5°N and 23.5°S) and southern extratropics (SET, south of
 738 23.5°S). The intercepts were set to zero since both variables are changes.

Region		Coefficient	Standard error (SE)	Lower 95%	Upper 95%
NET	Slope	2.135	0.235	1.674	2.596
TROP	Slope	1.385	0.753	-0.091	2.861
SET	Slope	1.809	0.552	0.728	2.891

739

740

741 Table 4: Maximum likelihood estimates of the relationship between the change in plant-
 742 available water ($\Delta\alpha$) and the change in mean temperature of the warmest month (ΔMTWA) by
 743 latitudinal bands for the northern extratropics (NET, north of 23.5°N), tropics (TROP, between
 744 23.5°N and 23.5°S) and southern extratropics (SET, south of 23.5°S). The intercepts were set
 745 to zero since both variables are changes.

Region		Coefficient	Standard error (SE)	Lower 95%	Upper 95%
NET	Slope	0.065	0.009	0.047	0.082
TROP	Slope	0.056	0.009	0.039	0.074
SET	Slope	0.052	0.011	0.031	0.073

746